Quantum phases of ultracold bosonic atoms in a one-dimensional optical superlattice

Arya Dhar*
Indian Institute of Astrophysics, II Block, Koramangala, Bangalore 560 034, India

Tapan Mishra†
Department of Physics, Georgetown University, Washington, DC 20057, USA

Ramesh V. Pai‡
Department of Physics, Goa University, Taleigao Plateau, Goa 403 206, India

B. P. Das§
Indian Institute of Astrophysics, II Block, Kormangala, Bangalore 560 034, India

(Received 2 March 2011; published 20 May 2011)

We analyze various quantum phases of ultracold bosonic atoms in a periodic one-dimensional optical superlattice. Our studies have been performed using the finite-size density-matrix renormalization group method in the framework of the Bose-Hubbard model. Calculations have been carried out for a wide range of densities and the energy shifts due to the superlattice potential. At commensurate fillings, we find the Mott insulator and the superfluid phases as well as Mott insulators induced by the superlattice. At a particular incommensurate density, the system is found to be in the superfluid phase coexisting with density oscillations for a certain range of parameters of the system.

DOI: 10.1103/PhysRevA.83.053621 PACS number(s): 03.75.Nt, 05.10.Cc, 05.30.Jp

I. INTRODUCTION

In a seminal paper in 1998, Jaksch *et al.* [1] extended the work of Fisher *et al.* [2] and predicted the superfluid–Mott insulator transition in ultracold bosonic atoms in an optical lattice. The observation of this transition in an optical lattice marked the beginning of the experimental studies of quantum phase transitions in ultracold atoms arising from strong correlations [3]. It also highlighted the possibility for detailed investigations of various kinds of strongly correlated quantum systems in optical lattices where the different parameters of these systems can be exquisitely controlled [4–7].

In this paper, we analyze the various quantum phases exhibited by ultracold bosonic atoms in a periodic one-dimensional optical superlattice using the finite-size density-matrix renormalization group (FSDMRG) method for certain parameters of the system. Previously, it has been shown using the exact diagonalization, quantum Monte Carlo, and the mean-field decoupling approximation methods that ultracold bosonic atoms in optical superlattices exhibit different phases, with various charge-density-wave orders apart from the usual superfluid (SF) and Mott insulator (MI) phases [8–10]. In the presence of a disordered and quasiperiodic potential, it has been shown that the system exhibits, in addition to SF and MI phases, the quasi-Bose glass and the incommensurate charge-density-wave phases [11,12]. In our present work, we vary the densities of the bosonic atoms from commensurate to incommensurate values for a relatively large value of the on-site interaction. The purpose of this investigation is to predict quantum phases that arise due to the influence of the superlattice in the parameter space that we have considered.

The paper is arranged in the following manner. The remainder of this section describes the model for bosonic atoms in the one-dimensional optical superlattice that we have chosen for our work. In Sec. II, the FSDMRG method and the quantities that we have calculated are briefly discussed. The results are presented in Sec. III, and our conclusions are summarized in Sec. IV.

An optical superlattice is formed by the superposition of two optical lattices of different frequencies (Fig. 1). Ultracold atoms in an optical superlattice can be described by a modified Bose-Hubbard model where the superlattice potential is explicitly included.

$$H = -t \sum_{\langle i,j \rangle} (\hat{a}_i^\dagger \hat{a}_j + \text{H.c.}) + \frac{U}{2} \sum_i \hat{n}_i(\hat{n}_i - 1) + \sum_i \lambda_i \hat{n}_i. \tag{1}$$

In the above equation, λ_i denotes the shift in the energy levels for each site due to the superlattice potential. For our work, we have considered an optical superlattice with the frequency of one optical lattice being double that of the other. Hence, the unit cell comprises two adjacent lattice sites as depicted in Fig. 1. As a result, $\lambda_i = \lambda$; $\forall\ i =$ odd integers, and $\lambda_i = 0$; $\forall\ i =$ even integers. In the first term of Eq. (1), $\langle i, j \rangle$ denotes a pair of nearest-neighbor sites i and j, t denotes the hopping amplitude between them, and $\hat{a}_i^\dagger(\hat{a}_i)$ is the creation (annihilation) operator, which creates (destroys) an atom at site i. In the second term of Eq. (1), U represents the on-site interatomic interaction, and $\hat{n}_i = \hat{a}_i^\dagger \hat{a}_i$ is the number operator. The Hamiltonian is rescaled in units of hopping amplitude t by setting $t = 1$ so that all the quantities becomes dimensionless.

*arya@iiap.res.in
†tapan@physics.georgetown.edu
‡rvpai@unigoa.ac.in
§das@iiap.res.in

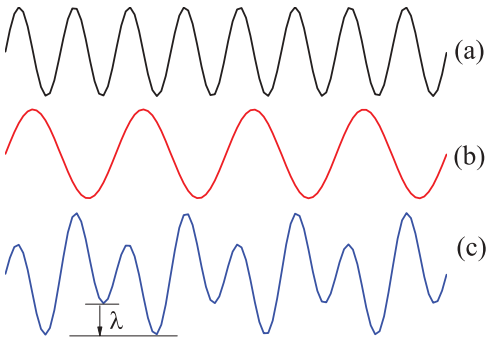

FIG. 1. (Color online) A superlattice [curve (c)] is formed by the superposition of two optical lattices [curves (a) and (b)], with the frequency of one being the double of the other. This results in an energy shift of λ for alternate sites.

In the absence of the superlattice potential, the model given in Eq. (1) reduces to the well-studied Bose-Hubbard model, which exhibits a transition from the gapless, compressible SF phase to the gapped, incompressible MI phase at integer densities [2]. However, for noninteger densities, the system remains in the superfluid phase.

The effect of the superlattice potential is to break the translational symmetry of the system. This leads to a change in the local (on site) chemical potential. In the present case, the local chemical potential changes at alternate sites in a periodic manner. The SF-MI transition has been predicted for such a system at integer fillings [10]. Apart from the SF phase, MI phases with various fillings at integer and half-integer densities have been predicted, depending on the relative values of the different parameters of the system [10,11]. The MI phase is characterized by a fixed number of atoms in a particular site or, more specifically, in a unit cell, and it occurs due to the strong on-site interaction between the atoms. In the two-period superlattice that we have considered, it is possible to have a new class of insulators in which alternate lattice sites occupy a fixed number of atoms. However unlike the MI phase, which is due to strong interatomic interactions, these insulators arise because of the superlattice potential. We therefore refer to these insulators as superlattice-induced Mott insulators (SLMI). If odd sites are occupied by one atom and there are none in the even ones, then we call it the SLMI-I phase; if odd sites are occupied by two atoms with none in the even sites, then it is called the SLMI-II phase.

II. METHOD OF CALCULATION

To obtain the ground-state wave function and the energy eigenvalues corresponding to model (1) for a system of N bosons in a lattice of length L, with on-site interactions and tunneling as well as the energy shift in alternate lattice sites due to the superlattice potential, we use the FSDMRG method with open boundary conditions [13,14]. This method is best suited for one-dimensional problems and has been successfully used to study the Bose-Hubbard model [14–18]. In our computations, we have considered four bosonic states per lattice site, and the weights of the states neglected in the density matrix formed from the left or the right blocks are less than 10^{-6} [16]. In order to improve the convergence, at the end of each DMRG step, we use the finite-size sweeping procedure given in [13,16]. To obtain the ground-state wave function $|\Psi_{LN}\rangle$ and the corresponding energy $E_L(N)$ for densities ranging from 0.24 to 1.25, we start with four sites and four atoms in the FSDMRG and increase both of them by two at each iteration until we have 24 atoms. Then we do not increase the number of atoms but increase the number of lattice sites to 100 by adding two sites in each DMRG iteration. After each step of the iteration, sweeping is done from left to right and also right to left across the entire lattice. This process is continued until the energy converges. The superlattice potential breaks the symmetry between the system and the environment. Therefore, it is necessary to perform the calculations on the system and the environment blocks separately at each DMRG iteration. Once the length $L = 100$ is reached, we keep it fixed and then increase the number of atoms by adding one at a time and perform a complete DMRG sweep for the convergence of the energy. This iterative procedure is continued until the number of bosons is equal to 125. By this process we obtain the wave functions and the corresponding energies of model (1) for densities ranging from 0.24 to 1.25. We have carried out the calculations for a range of values of λ from 0 to 15, with t and U fixed at 1.0 and 10.0, respectively.

Using the ground-state wave function $|\Psi_{LN}\rangle$ and the corresponding energy $E_L(N)$, the following quantities are calculated to identify the various phases exhibited by the system. First, the chemical potential of a system for the density $\rho = N/L$ is defined as follows:

$$\mu = \frac{\delta E_L(N)}{\delta N}. \tag{2}$$

The gapped and gapless phases are distinguished from the behavior of ρ as a function of μ [19]. To get information about the on-site density distribution in various phases exhibited by the system, we calculate the on-site density $\langle n_i \rangle$, which is defined as

$$\langle n_i \rangle = \langle \Psi_{LN} | \hat{n}_i | \Psi_{LN} \rangle. \tag{3}$$

The momentum distribution $n(k)$ and the structure function $S(k)$ are defined as the Fourier transform of the single-particle density matrix $\langle \hat{a}_p^\dagger \hat{a}_q \rangle = \langle \Psi_{LN} | \hat{a}_p^\dagger \hat{a}_q | \Psi_{LN} \rangle$ and the density-density correlation function $\langle \hat{n}_p \hat{n}_q \rangle = \langle \Psi_{LN} | \hat{n}_p \hat{n}_q | \Psi_{LN} \rangle$, respectively:

$$n(k) = \frac{1}{L} \sum_{p,q} e^{ik(p-q)} \langle \hat{a}_p^\dagger \hat{a}_q \rangle, \tag{4}$$

$$S(k) = \frac{1}{L} \sum_{p,q} e^{ik(p-q)} \langle \hat{n}_p \hat{n}_q \rangle. \tag{5}$$

The momentum distribution, $n(k)$ will indicate the presence of a SF phase in the system. The structure function will give information about the presence of any density-wave order in the system and also the effect of superlattice potential on the Brillouin zone boundaries.

To get an idea of the various gapped and gapless phases in the system, we plot the density ρ versus the average chemical potential μ. However to draw the phase diagram, we need accurate values of the chemical potential, and hence, we calculate the chemical potential (both μ^+ and μ^-) in the

thermodynamic limit $L \to \infty$. μ_L^+ is defined as the difference in the energy of the system of length L if one atom is added to the system, whereas μ_L^- is the energy cost when one atom is removed from the system, i.e., $\mu_L^+ = E_L(N+1) - E_L(N)$ and $\mu_L^- = E_L(N) - E_L(N-1)$. We plot these chemical potential values versus the reciprocal of the length $(1/L)$ and then extrapolate to length tending to infinity $(1/L \to 0)$ to get the values of the chemical potential in the thermodynamic limit. We plot these chemical potential values for both density equal to 0.5 and 1.0 for different superlattice potentials λ to get the phase diagram.

III. RESULTS AND DISCUSSION

Before we discuss the details of our results, we first summarize the main features of the phase diagram. It is well established that bosons in a normal optical lattice, described by the Bose-Hubbard model [2], exhibit the superfluid to Mott insulator quantum phase transition at some critical value of U for integer densities. (For example, for $\rho = 1$ this transition occurs at the critical on-site interaction $U_C \sim 3.4$ [15,16] in one dimension). For noninteger densities, only the superfluid phase exists in the ground state. The Mott insulator phase has a finite gap and is incompressible. On the other hand, the superfluid phase is gapless and compressible. When we include the superlattice potential, the energy levels at each site are shifted by λ_i, and this leads to the additional incompressible, gapped SLMI phase. In model (1), the SLMI phase occurs at commensurate densities, i.e., when ρ is equal to an integer or a half integer, because the superlattice that we have considered in our calculations has a periodicity of two lattice sites. For $\rho = 1/2$, we observe a SF to SLMI-I phase transition as the strength of the superlattice potential is increased. However, for $\rho = 1$ we get the MI and the SLMI-II phases along with a SF phase sandwiched between them. Such a transition at $\rho = 1.0$ had already been predicted in an optical superlattice [8] using a quantum Monte Carlo approach. However, this SF phase at $\rho = 1$ is not the usual SF phase that arises due to a large value of t/U. In fact, in our present case, the ratio is very small $(t/U \sim 0.1)$. This SF phase is a result of the competition between the superlattice potential λ and the on-site repulsive interaction potential U. Moreover, because of the superlattice potential, this SF phase will have finite density modulations.

We first discuss the results for commensurate densities and then for incommensurate densities. In Fig. 2 we plot ρ versus μ, defined by Eq. (2), for a fixed value of $U = 10$ but with λ varying from 0 to 15. The gapped phases show up in this type of plot as plateaus with the gap G_L equal to the width of the plateau, i.e., $G_L = \mu_L^+ - \mu_L^-$, where μ_L^+ and μ_L^- are the values of the chemical potential at the upper and lower knees of the plateau, respectively.

In Fig. 2 we see for $\lambda = 0$ that there exists only one plateau at $\rho = 1.0$, corresponding to the MI phase, which is expected since the value of U is very large compared to t [16]. This MI phase survives for small values of λ. As the strength of λ increases, two interesting features appear in the plots: (i) a new plateau appears at $\rho = 1/2$, and (ii) the width of the plateau at $\rho = 1$ decreases. This can be clearly seen in the plots of ρ versus μ for various λ values, as shown in Fig. 3. For $\lambda = 0.2$, the gapped phase exists only at $\rho = 1$ (Fig. 3) and is gapless

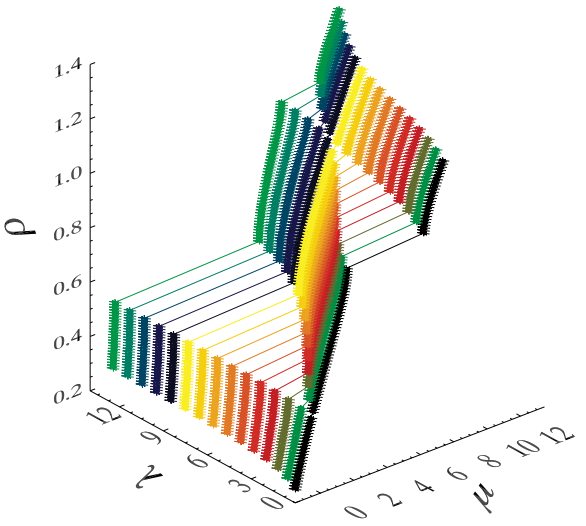

FIG. 2. (Color online) Density ρ plotted against the chemical potential for various values of λ at a fixed $U = 10$ and $t = 1$.

at $\rho = 1/2$. As λ is increased beyond 0.8, two gapped phases appear, at $\rho = 1/2$ and $\rho = 1$. The gapped phase at $\rho = 1/2$ occurs due to the transition from the SF to the SLMI-I phase with one atom per unit cell, occupying alternate sites.

For λ values between 0.8 and 9.6, the system exhibits two gapped regions, one at $\rho = 1/2$ and the other at $\rho = 1$. The gap at $\rho = 1/2$ increases steadily as λ increases and remains finite. On the other hand, for values of $\lambda > 0.0$, the gap at $\rho = 1$ decreases continuously and ultimately vanishes at around $\lambda = 9.6$. This kind of behavior for $\rho = 1$ is due to the competition between the superlattice potential λ and on-site repulsive interaction U. The on-site interaction U tries to impose the MI phase in the system, whereas λ tends to introduce the SLMI-II phase. As long as U is greater than λ, the MI phase is energetically favorable for $\rho = 1$ resulting in a finite gap. As λ becomes comparable to the value of U (in this calculation we have fixed $U = 10$), neither the MI phase, with one boson at every site, nor the SLMI-II phase, with two bosons at every alternate site, is energetically favorable.

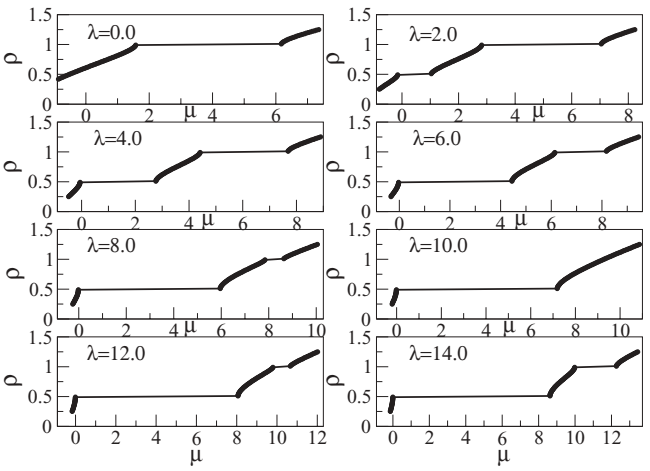

FIG. 3. The chemical potential μ plotted against density ρ for various values of λ, with $U = 10$.

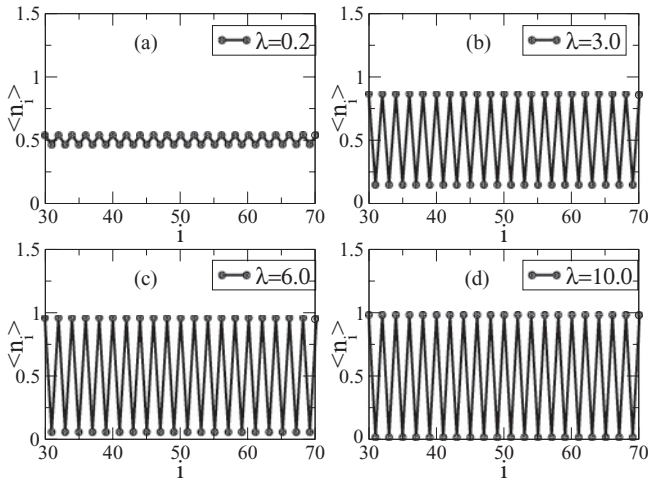

FIG. 4. On-site number density plotted against lattice site index at density $\rho = 0.5$.

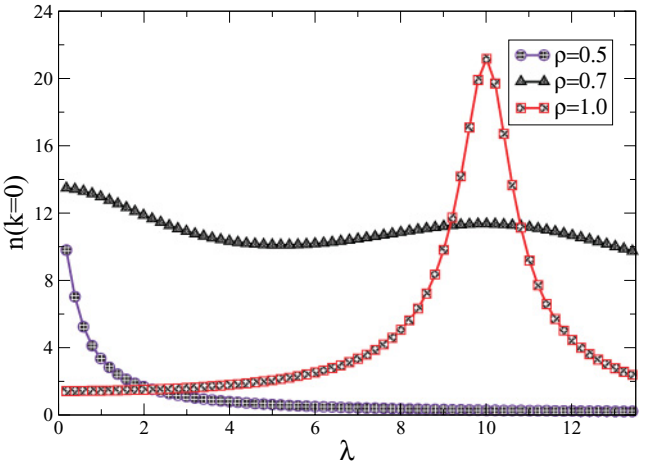

FIG. 6. (Color online) Momentum distribution $n(k = 0)$ plotted against various values of λ for densities $\rho = 0.5$,0.7, and 1.0.

This leads to the vanishing of the energy gap, and the system becomes a SF.

When λ is larger than the value of U, the superlattice potential dominates over the on-site interaction. As a result, the gap at $\rho = 1$ opens up again, which can be seen clearly from Figs. 2 and 3. This gap is due to the system being in the SLMI-II phase. The regions other than commensurate densities, i.e., $\rho = 1/2$ and 1, remain in the gapless SF phase for all values of λ.

To confirm the above findings concerning the existence of the MI and the SLMI phases, we plot the on-site average number density $\langle \hat{n}_i \rangle$ with respect to the site index i as shown in Figs. 4 and 5 for $\rho = 1/2$ and 1, respectively. For values of λ less than 0.8, there are no oscillations at density equal to 0.5. However, as the value of λ is increased, the density oscillations begin to set in the system, and at higher values of λ, a clear $\{101010\cdots\}$ occupancy configuration can be seen, confirming the presence of a SLMI-I phase (Fig. 4). At $\rho = 1$, for low values of λ, Fig. 5 shows a constant number density equal to 1.0, implying the MI phase. As λ is increased but is less than 9.6, the superlattice potential induces some oscillations, but the system is still in the MI phase. Even at $\lambda = 10.0$, the oscillations vary from 1.5 (maximum) to 0.5 (minimum), significantly different from the SLMI-II configuration of $\{202020\cdots\}$. Once λ becomes much larger than U, the SLMI-II configuration is observed. For example, at values of $\lambda = 14$, the number occupancy in the sites looks very similar to the SLMI-II configuration, as can be seen from Fig. 5.

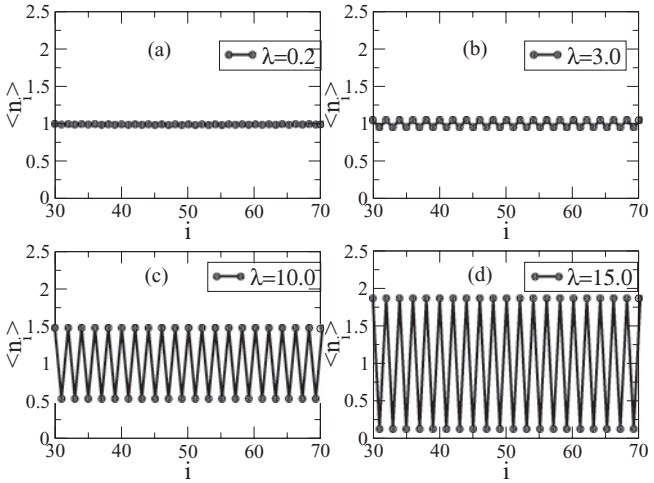

FIG. 5. On-site number density plotted against lattice site index at density $\rho = 1.0$.

The momentum distribution is then calculated using Eq. (4). The value of $n(k)$ at $k = 0$ is plotted against λ for three different values of ρ (0.5, 0.7, and 1.0). A finite value of $n(k)$ at $k = 0$ is a signature of the SF phase in the system. These plots are compared with the chemical potential versus ρ plots (Fig. 2) to confirm the gapped and gapless phases. In Fig. 6, for $\rho = 0.5$, $n(k = 0)$ has a very high value when λ is smaller than 0.8, which signifies the SF phase. As λ increases beyond 0.8, $n(k = 0)$ falls off to values very close to zero, implying certain phase transition from the SF phase to an insulating phase. This insulating phase is the SLMI-I, as confirmed from the $\langle \hat{n}_i \rangle$ plots (Fig. 4). For $\rho = 1$, $n(k = 0)$ starts with values very close to zero (Fig. 6). Due to the very high value of U, the system resides in the MI state. As λ becomes comparable to U, $n(k = 0)$ attains a finite peak value, thus implying the transition from the MI to the SF phase. This result is in agreement with the ones obtained from the chemical potential plots (Figs. 2 and 3). As λ is increased further, $n(k = 0)$ again drops to values very close to zero, implying another phase transition, but this time the transition is from SF to SLMI-II. Hence, it can be said that this SF is not the usual SF that comes due to t/U ratio but is a consequence of the competition between the parameters U and λ. At incommensurate densities, for example, $\rho = 0.7$ (Fig. 6), it is observed that $n(k = 0)$ stays finite for all values of λ, without any signs of it vanishing, showing the presence of a SF phase throughout the values of λ considered in this work.

Figures 7–9 give the structure function as a function of k for various values of density ($\rho = 0.5$, 1.0, and 0.7, respectively). In the normal optical lattice, the periodicity is one lattice site. So for a MI phase, the structure function peaks at $k = \pm 2\pi$

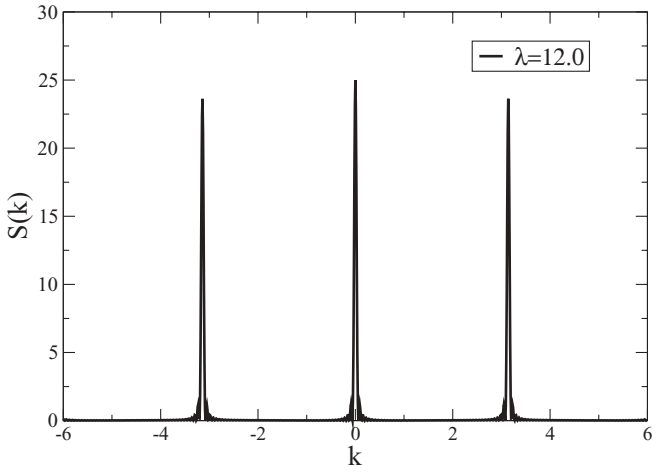

FIG. 7. Structure function $S(k)$ vs the momentum k for density of 0.5.

[20]. However, in an optical superlattice, the periodicity is doubled. As a result, the Brillouin zone is halved. Hence, in the MI phase for an optical superlattice, we expect to observe the peaks of $S(k)$ at $k = \pm\pi$. It can also be observed that for $\rho = 1$, the peaks do not appear for lower values of λ (Fig. 8). The onset of the peaks actually signify the effects of the superlattice potential λ in the system [8], thus changing the Brillouin zone boundaries. From Fig. 7, we see two well-defined peaks at $k = \pm\pi$ for $\rho = 0.5$ at a very large value of λ, implying the presence of a SLMI-I phase. At $\rho = 0.7$, we see two peaks at $k = \pm\pi$ for λ more than $\approx$2.0. This is a consequence of some density oscillations induced in the system by the superlattice potential.

The value of the structure function at $k = \pi$ is plotted in Fig. 10 for some fixed densities against λ to see how the effect of superlattice potential evolves in the system. For $\rho = 0.5$, $S(\pi)$ starts from very close to zero, increases steadily, and then becomes almost constant. For $\rho = 1$, initially, there is no peak in the $S(k)$ plot at $k = \pi$. As λ is increased, even in the MI phase, we see a finite value of the structure function at $k = \pi$, indicating the onset of the effect of the superlattice potential.

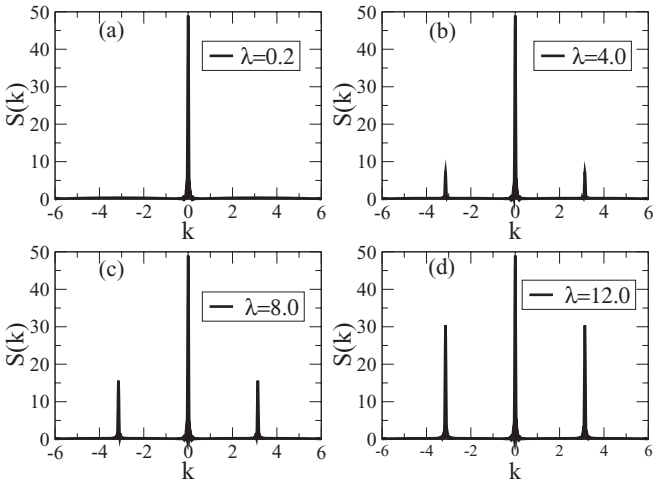

FIG. 8. Structure function $S(k)$ vs the momentum k for density of 1.0 for different values of λ.

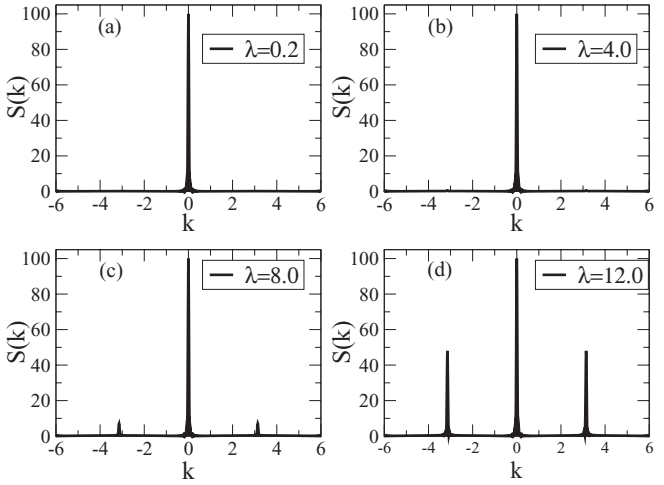

FIG. 9. Structure function $S(k)$ vs the momentum k for density of 0.7 for different values of λ.

Once λ overcomes U, the value of $S(\pi)$ increases rapidly, showing the onset of the SLMI-II phase. It is also noted that, at $\lambda \approx 10$, $S(k = \pi)$ is finite, showing some density modulations in the system. As seen earlier, at the above value of λ, the system undergoes a transition from the MI to the SF phase. Thus, the SF at $\rho = 1.0$ coexists with a finite density oscillation in the system. For $\rho = 0.7$, $S(\pi)$ is very close to zero for low values of λ and then increases as λ becomes greater than some value and then goes on increasing, implying the setting in of some density modulations in the system. Hence, finite peaks of $S(k)$ at $k = \pi$ (Fig. 9) for $\rho = 0.7$ imply the effect of superlattice potential in the system bringing about density modulation, although the system is in a superfluid phase, as indicated in the $n(k = 0)$ plot (Fig. 6) for all values of λ. So we see a coexistence of SF and some sort of density oscillations in the system at the incommensurate density of 0.7.

The phase diagram in the μ-λ plane for $U = 10$ is presented in Fig. 11. The phase diagram consists of SF, MI, SLMI-I, and SLMI-II phases, depending on the density and the superlattice potential.

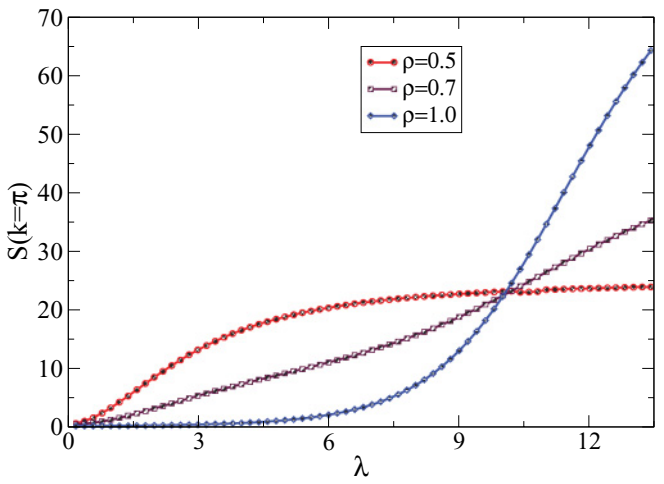

FIG. 10. (Color online) S($k = \pi$) vs λ for three different density values, $\rho = 0.5, 0.7$, and 1.0.

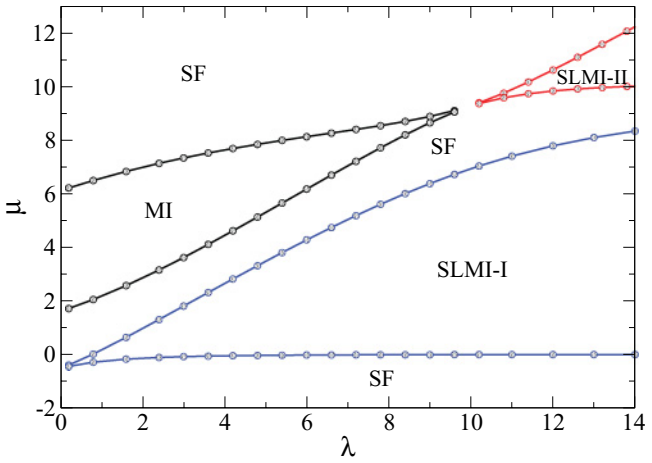

FIG. 11. (Color online) Phase diagram for the system of an optical superlattice.

IV. CONCLUSION

We have analyzed the various phases exhibited by a system of bosons in an optical superlattice with a unit cell consisting of two lattice sites using the FSDMRG method for a large value of the on-site interaction U. We found that, at density $\rho = 1/2$, the system is initially in the gapless superfluid phase. But as the value of the superlattice potential λ is increased, a finite gap arises, which corresponds to the SLMI-I phase corresponding to the configuration [1 0 1 0$\cdots$]. At integer density, $\rho = 1$, the system is initially in the gapped MI phase because of the large value of U. But as the superlattice potential value is increased, the gap keeps on decreasing and ultimately shrinks to zero when $\lambda \approx U$. This gapless SF phase coexists with a finite $S(k = \pi)$ in the system, implying density oscillations. As the value of λ is further increased, the gap reopens, corresponding to the SLMI-II phase, with a configuration [2 0 2 0$\cdots$]. At the incommensurate density, $\rho = 0.7$, we find the simultaneous existence of the SF phase along with density oscillations in the system.

ACKNOWLEDGMENTS

R.V.P. acknowledges financial support from CSIR and DST, India. We are grateful to William Phillips, Yoshiro Takahashi, Mikhail Baranov, Gora Shlyapnikov, Arun Paramekanti and Marcos Rigol for stimulating discussions.

[1] D. Jaksch, C. Bruder, J. I. Cirac, C. W. Gardiner, and P. Zoller, Phys. Rev. Lett. **81**, 3108 (1998).
[2] M. P. A. Fisher, P. B. Weichman, G. Grinstein, and D. S. Fisher, Phys. Rev. B **40**, 546 (1989).
[3] M. Greiner, O. Mandel, T. Esslinger, T. W. Hansch, and I. Bloch, Nature (London) **415**, 39 (2002).
[4] M. Lewenstein, A. Sanpera, V. Ahufinger, B. Damski, A. Sen(De), and U. Sen, Adv. Phys. **56**, 243 (2007).
[5] I. Bloch, Nature (London) **453**, 1016 (2008).
[6] I. Bloch, J. Dalibard, and W. Zwerger, Rev. Mod. Phys. **80**, 885 (2008).
[7] V. I. Yukalov, Laser Phys. **19**, 1 (2009).
[8] V. G. Rousseau, D. P. Arovas, M. Rigol, F. Hebert, G. G. Batrouni, and R. T. Scalettar, Phys. Rev. B **73**, 174516 (2006).
[9] R. Roth and K. Burnett, Phys. Rev. A **68**, 023604 (2003).
[10] B.-L. Chen, S.-P. Kou, Y. Zhang, and S. Chen, Phys. Rev. A **81**, 053608 (2010).
[11] F. Schmitt, M. Hild, and R. Roth, J. Phys. A **43**, 235301 (2010).
[12] G. Roux, T. Barthel, I. P. McCulloch, C. Kollath, U. Schollwöck, and T. Giamarchi, Phys. Rev. A **78**, 023628 (2008).
[13] S. R. White, Phys. Rev. Lett. **69**, 2863 (1992); Phys Rev. B **48**, 10345 (1993).
[14] U. Schollwöck, Rev. Mod. Phys. **77**, 259 (2005).
[15] T. D. Kuhner and H. Monien, Phys. Rev. B **58**, R14741 (1998).
[16] R. V. Pai and R. Pandit, Phys. Rev. B **71**, 104508 (2005).
[17] T. D. Kuhner, S. R. White, and H. Monien, Phys. Rev. B **61**, 12474 (2000).
[18] L. Urba *et al.*, J. Phys. B **39**, 5187 (2006).
[19] S. Ramanan, T. Mishra, M. S. Luthra, R. V. Pai, and B. P. Das, Phys. Rev. A **79**, 013625 (2009).
[20] V. W. Scarola, E. Demler, and S. Das Sarma, Phys. Rev. A **73**, 051601(R) (2006).